



CERN-EP-2022-059  
22 March 2022

## Study of charged particle production at high $p_T$ using event topology in pp, p–Pb and Pb–Pb collisions at $\sqrt{s_{NN}} = 5.02$ TeV

ALICE Collaboration

### Abstract

This letter reports measurements which characterize the underlying event associated with hard scatterings at mid-pseudorapidity ( $|\eta| < 0.8$ ) in pp, p–Pb and Pb–Pb collisions at centre-of-mass energy per nucleon pair,  $\sqrt{s_{NN}} = 5.02$  TeV. The measurements are performed with ALICE at the LHC. The hard scatterings are identified by the leading particle defined as the charged particle with the largest transverse momentum ( $p_T$ ) in the collision and having  $8 < p_T < 15$  GeV/ $c$ . The  $p_T$  spectra of associated particles ( $0.5 \leq p_T < 6$  GeV/ $c$ ) are measured in different azimuthal regions defined with respect to the leading particle direction: toward, transverse, and away. The associated charged particle yields in the transverse region are subtracted from those of the away and toward regions. The remaining jet-like yields are reported as a function of the multiplicity measured at forward rapidities. The measurements show a suppression of the jet-like yield in the away region and an enhancement of high- $p_T$  associated particles in the toward region in central Pb–Pb collisions, as compared to minimum-bias pp collisions. These observations are consistent with previous measurements that used two-particle correlations, and with an interpretation in terms of parton energy loss in a high-density quark gluon plasma. These yield modifications vanish in peripheral Pb–Pb collisions and are not observed in either high-multiplicity pp or p–Pb collisions.

arXiv:2204.10157v1 [nucl-ex] 21 Apr 2022

## 1 Introduction

In proton-proton (pp) collisions, jets, originating from partonic scatterings with large momentum transfer, are accompanied by particles produced by initial- and final-state radiation (ISR and FSR, respectively), as well as, by a plethora of other mechanisms. These include proton break-up, and, in a scenario incorporating multi-parton interactions (MPI) [1, 2], several semi-hard parton-parton scatterings in a single pp collision. These jet-accompanying particles experimentally make up the underlying event (UE) and are commonly studied via azimuthal separations from the jets to minimise the influence of hard scatterings. The present study follows the strategy originally introduced by the CDF collaboration [3]. First, the leading charged particle in the event is found, i.e., the charged particle with the highest transverse momentum in the collision ( $p_T^{\text{trig}}$ ). Secondly, the associated particles ( $p_T < p_T^{\text{trig}}$ ) are measured in three topological regions depending on their azimuthal angle relative to the leading particle,  $|\Delta\phi| = |\phi^{\text{assoc}} - \phi^{\text{trig}}|$ , see Fig. 1.

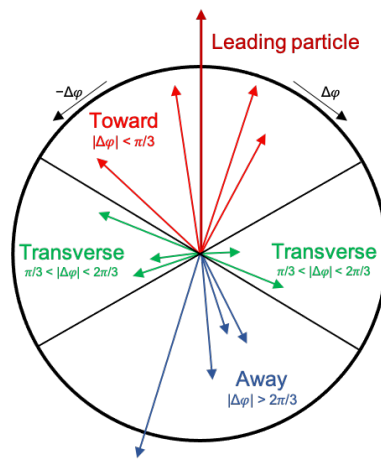


Figure 1: (colour online) Illustration of toward, away and transverse regions with respect to the leading particle in a collision.

The toward region contains the primary jet within the acceptance of the detector, while the away region contains the back-scattered particles of the recoil jet [4]. In contrast, the transverse region is dominated by the underlying-event dynamics, but it also includes contributions from ISR and FSR [5].

The measurements performed at RHIC and LHC in small systems (pp, p–A, and d–A collisions) have shown for high particle multiplicities similar phenomena as were originally observed only in A–A collisions and have been attributed there to the formation of the strongly interacting quark gluon plasma [6, 7], namely, long range angular correlations and collectivity [8]. The origin of these effects in small systems is still an open question; on one hand, hydrodynamical calculations describe some aspects of the data [9]; on the other hand, mechanisms like colour reconnection [10], rope hadronisation [11], and string shoving [12] can produce collective-like effects in Monte Carlo event generators such as PYTHIA 8 [13]. Thus, investigating pp collisions as a function of the charged particle multiplicity has become ever more pertinent [9, 14–18]. The interpretation of the results from the analysis of high-multiplicity pp collisions is challenging due to the selection biases of the sample towards events in which partonic scatterings with large momentum transfer (hard scatterings) occurred. To mitigate this inherent bias, Martin *et al.* [19] suggested to use the charged-particle multiplicity in the transverse region ( $N_{\text{ch}}^T$ ) as a classifier of the activity in the collisions, since the correlation between  $N_{\text{ch}}^T$  and the hardest scattering in the collision is small. The ALICE collaboration has reported the first  $N_{\text{ch}}^T$  spectra measured in pp collisions at centre-of-mass energy,  $\sqrt{s} = 13$  TeV [20]. Event generators, such as PYTHIA 8 [13] and EPOS-LHC [21], do not provide a good description of the measured distribution of the ratio  $N_{\text{ch}}^T / \langle N_{\text{ch}}^T \rangle$ , where  $\langle N_{\text{ch}}^T \rangle$  is the event-averaged charged-particle multiplicity in the transverse region, underestimating in particular

the number of collisions with large  $N_{\text{ch}}^T$  ( $> 3 \times \langle N_{\text{ch}}^T \rangle$ ). In the framework of MPI-based models, like those implemented in PYTHIA 8 and HERWIG 7 [22], the probability for a hard scattering in the collision increases with decreasing impact parameter<sup>1</sup> between the colliding protons. Thus, requiring a high- $p_T$  particle (e.g.,  $p_T^{\text{trig}} > 8 \text{ GeV}/c$ ) in a given pp collision biases the selection of collisions towards those with a smaller impact parameter [23], which in turn biases the selection towards pp collisions with more MPI [20]. This feature of the  $N_{\text{ch}}^T$ -based analysis is important for the isolation of potential MPI and colour reconnection effects, which according to PYTHIA 8, produce effects resembling collective behaviour [10]. By construction, MPI and colour reconnection effects are expected to be more relevant in the transverse region than in the away and toward regions [24]. It is worth mentioning that the MPI picture has been used to explain the  $p_T$  spectra in p–Pb collisions and peripheral Pb–Pb collisions [25–27]. Studies, as a function of  $N_{\text{ch}}^T$ , are therefore important to the understanding of the effects observed in high-multiplicity pp collisions. Last but not least, measurements of UE observables are also important to tune event generators [28] that include hard partonic scatterings and MPI.

This letter reports the inclusive charged-particle transverse momentum spectra in pp, p–Pb and Pb–Pb collisions at centre-of-mass energy per nucleon pair  $\sqrt{s_{\text{NN}}} = 5.02 \text{ TeV}$  containing a high- $p_T$  leading particle within the kinematic intervals  $8 \leq p_T^{\text{trig}} < 15 \text{ GeV}/c$  and  $|\eta| < 0.8$ . This guarantees the selection of collisions in which the average activity in the transverse region is roughly flat as a function of  $p_T^{\text{trig}}$  [20], and therefore, any additional selection on the charged particle multiplicity will only modulate the UE activity. The  $p_T$  spectra of associated charged particles ( $0.5 \leq p_T < 6 \text{ GeV}/c$  and  $|\eta| < 0.8$ ) are measured in the toward, away, and transverse regions as a function of the average charged particle multiplicity. The measurements are performed considering different event classes defined in terms of the multiplicity registered in the forward detectors. To further investigate the possible modification of the particles produced in the hard scattering in pp, p–Pb, and Pb–Pb collisions, the  $p_T$  distributions in the toward ( $dN_{\text{ch}}^t/dp_T$ ) and away ( $dN_{\text{ch}}^a/dp_T$ ) regions obtained after the subtraction of the  $p_T$  spectra in the transverse region ( $dN_{\text{ch}}^T/dp_T$ ) are also reported. The subtracted yields ( $dN_{\text{ch}}^{\text{st,sa}}/dp_T$ ) are further normalised to those measured in minimum-bias (MB) pp collisions,

$$I_X^{\text{t,a}} \equiv \frac{(dN_{\text{ch}}^{\text{t,a}}/dp_T - dN_{\text{ch}}^T/dp_T)|_X}{(dN_{\text{ch}}^{\text{t,a}}/dp_T - dN_{\text{ch}}^T/dp_T)|_{\text{pp,MB}}} = \frac{(dN_{\text{ch}}^{\text{st,sa}}/dp_T)|_X}{(dN_{\text{ch}}^{\text{st,sa}}/dp_T)|_{\text{pp,MB}}}, \quad (1)$$

where  $X$  indicates the collision system and the event multiplicity class. In this way, the hard process  $p_T$  spectra in the toward and away regions are isolated, and thus allowing us to study possible modifications to the produced particles due to medium effects in high-multiplicity pp, p–Pb, and Pb–Pb collisions. In heavy-ion collisions, this ratio is sensitive to the same effects which were studied using the  $I_{\text{AA}}$  quantity [29–31], where jets produced in the early stage of the collision propagate through the hot and dense quark–gluon plasma. Their interaction with the coloured medium lead to parton-energy loss (jet quenching) [32] which, for example, results in the suppression of the charged-particle yield at high  $p_T$  [33], and the suppression of the high- $p_T$  yield in the away region [29, 30]. It is worth mentioning that jet quenching effects have not been observed so far in small systems [33, 34].

## 2 Experiment and data analysis

This analysis is based on the data recorded by the ALICE apparatus during the pp and Pb–Pb runs at  $\sqrt{s_{\text{NN}}} = 5.02 \text{ TeV}$  in 2015, and the p–Pb run at  $\sqrt{s_{\text{NN}}} = 5.02 \text{ TeV}$  in 2016. The present study uses the V0 detector, and the Silicon Pixel Detector (SPD) for triggering and background rejection. The V0 consists of two arrays of scintillating tiles placed on each side of the interaction point covering the full azimuthal acceptance and the pseudorapidity intervals of  $2.8 < \eta < 5.1$  (V0A) and  $-3.7 < \eta < -1.7$  (V0C). The SPD is the innermost part of the Inner Tracking System (ITS) and it is the closest detector

<sup>1</sup>In event generators like PYTHIA 8 the impact parameter profile is described by an overlap matter distribution of the two incoming hadrons.

to the interaction point. It consists of two cylindrical silicon pixel layers at radial distances of 3.9 and 7.6 cm from the beam line and the pseudorapidity coverages of the two layers are  $|\eta| < 2$  and  $|\eta| < 1.4$ , respectively. The data were collected using a minimum-bias trigger, which required a signal in both VOA and VOC detectors. The offline event selection was optimised to reject beam-induced background in all collision systems by utilising the timing signals in the two V0 detectors. In Pb–Pb collisions, the beam-induced background is further suppressed by correlating the timing signals of the neutron zero degree calorimeters, which are positioned on both sides of the interaction point at 112.5 m distance along the beam axis [35]. The signals from the zero degree calorimeters are also used to suppress the contamination from electromagnetic interactions. A criterion based on the offline reconstruction of multiple primary vertices in the SPD is applied to reduce the pileup caused by multiple interactions in the same bunch crossing [36]. The results presented in this letter are for minimum-bias triggered pp collisions having at least one charged particle in the pseudorapidity interval  $|\eta| < 1$  (INEL>0). The INEL>0 event class corresponds to about 75% of the total inelastic cross section [37]. For pp and Pb–Pb collisions, the sample is subdivided into different multiplicity classes based on the total charge deposited in both V0 sub-detectors, which is termed as V0M amplitude [38]. For p–Pb collisions, the sample is subdivided based on the total charge deposited in VOA sub-detector (VOA amplitude) [39], which is located in the Pb-going direction. To ensure that a hard scattering took place in the collision, events are required to have a trigger particle within  $8 \leq p_T^{\text{trig}} < 15$  GeV/c. The total number of analysed collisions before the trigger particle selection are about  $10^8$ ,  $10^8$ , and  $10^7$  for pp, p–Pb, and Pb–Pb collisions, respectively.

The transverse momentum of particles is determined from measurements in the central barrel with the ITS and the Time Projection Chamber (TPC). The ITS is a tracking detector which consists of six cylindrical layers of silicon detectors. The TPC is a cylindrical drift detector which covers a radial distance of 85–247 cm from the beam axis and it has longitudinal dimension extending from about -250 cm to +250 cm around the nominal interaction point. Primary charged particles are measured in the pseudorapidity range of  $|\eta| < 0.8$  and with  $p_T > 0.5$  GeV/c. The particles with mean proper lifetime larger than 1 cm/c, which are either produced directly in the interaction or from decays of particles with mean proper lifetime smaller than 1 cm/c are termed as primary particles [40]. The track selection follows a procedure similar to the one described in Ref. [41] and only few specific details are reported here. Tracks are required to have two hits in the ITS, out of which at least one should be in either of the two innermost layers. The geometrical track length  $L$  is calculated in the TPC readout plane, excluding the information from the pads at the sector boundaries ( $\approx 3$  cm from the sector edges). The trajectory lengths built from radial segments, i.e. the crossed TPC pad rows, traversed in the TPC by a particle are required to be larger than 85% of the geometrical track length. The pad rows are made of at least 3 neighbouring individual observations (clusters), and their height varies from 7.5 mm to 15 mm [42]. The trajectory lengths built from clusters (one cluster per pad row) is required to be larger than  $0.7 \times L$ . The fraction of TPC clusters shared with another track is required to be lower than 0.4. The fit quality for the ITS and TPC track points must satisfy  $\chi_{\text{ITS}}^2/N_{\text{hits}} < 36$  and  $\chi_{\text{TPC}}^2/N_{\text{clusters}} < 4$ , respectively, where  $N_{\text{hits}}$  and  $N_{\text{clusters}}$  are the numbers of hits in the ITS and the number of clusters in the TPC, respectively. Only tracks with  $\chi_{\text{TPC-ITS}}^2 < 36$  are included in the analysis, where  $\chi_{\text{TPC-ITS}}^2$  is calculated comparing the track parameters from the combined ITS and TPC track reconstruction to that derived only from the TPC and constrained to the interaction point. The definition of  $\chi_{\text{TPC-ITS}}^2$  can be found in Ref. [43]. To reduce the contamination from secondary particles, tracks are accepted if their distance-of-closest-approach (DCA) to the reconstructed primary interaction vertex satisfies in the longitudinal ( $d_z$ ) and transverse ( $d_{xy}$ ) directions the conditions  $d_z < 2$  cm and  $d_{xy} < 0.018$  cm +  $0.035$  cm  $\times$  (GeV/c)  $\times p_T^{-1.0}$ .

The measurement of the transverse momentum spectra of charged particles follows the standard procedure of the ALICE collaboration [41, 44]. The raw yields are corrected for efficiency and contamination from secondary particles. The efficiency correction is calculated from Monte Carlo simulations with GEANT3 [45] transport code, which made use of PYTHIA 8 (Monash) [28], EPOS-LHC [21] and HIJING [46] event generators for pp, p–Pb and Pb–Pb collisions, respectively and incorporated a detailed

description of the detector material, geometry and response. Since the event generators do not reproduce the relative abundances of different particle species in the real data, the efficiency obtained from the simulations is re-weighted considering the particle composition from data as outlined in [41]. A multi-component template fit based on the DCA distributions from the simulation is used for the estimation of secondary contamination [41].

The  $p_T$  spectra for the toward and away regions include contributions from the jet fragmentation, ISR, and FSR, as well as, the contribution from the underlying event. In order to increase the sensitivity to the hardest process of the event, the particle yields measured in the transverse region are subtracted from the corresponding yields in both the toward and away regions:  $dN_{\text{ch}}^{\text{t,a}}/dp_T - dN_{\text{ch}}^{\text{T}}/dp_T$ . This approach assumes that the background (UE, ISR, and FSR) in the toward and away regions is similar to the activity in the transverse region. However, one has to keep in mind that in Pb–Pb collisions two-particle correlations are affected by anisotropic transverse flow. In particular, the main contribution is due to the elliptic flow,  $v_2$ , which is the second order coefficient in the Fourier expansion of the azimuthal distribution of the particle momenta [47]. This elliptic azimuthal anisotropy modulates the background according to:

$$B(\Delta\phi) = B_0(1 + 2V_2 \cos(2\Delta\phi)), \quad (2)$$

where  $V_2$  is approximately given by the product of anisotropic flow coefficients for trigger and associated particles at their respective momenta i.e.  $V_2 \approx v_2^{\text{trig}} v_2^{\text{assoc}}$ . The existing  $v_2$  measurements over a broad transverse momentum range [48] suggest that the effect of the  $v_2$  modulation of background should be more relevant in semi-central Pb–Pb collisions. The effect is expected to be important at low and intermediate transverse momenta and decreases for high transverse momentum particles [30]. In the high- $p_T$  region of interest for the jet quenching studies, namely  $p_T > 4 \text{ GeV}/c$ , the effect of the  $v_2$  modulation is estimated to be small (about 5%) for Pb–Pb collisions. Given that the  $v_2$  effect is larger in Pb–Pb collisions than in pp and p–Pb collisions, no correction for the  $v_2$  modulation is applied for these collision systems since its effect is smaller than the other sources of systematic uncertainty.

The results are shown as a function of the average number of charged particles in the transverse region  $\langle N_{\text{ch}}^{\text{T}} \rangle$ . The values of  $\langle N_{\text{ch}}^{\text{T}} \rangle$  are extracted in each multiplicity class from the raw  $N_{\text{ch}}^{\text{T}}$  distributions which are corrected for detector effects using a Bayesian unfolding [49]. As a crosscheck, the  $\langle N_{\text{ch}}^{\text{T}} \rangle$  values are also calculated by integrating the transverse momentum distributions in the interval  $0.5 \leq p_T < 8 \text{ GeV}/c$ . The difference between the results from the two strategies is assigned as the systematic uncertainty on  $\langle N_{\text{ch}}^{\text{T}} \rangle$ .

The systematic uncertainties related to the track selection criteria were studied by repeating the analysis varying one-by-one the track selection criteria [41, 44]. In particular, the upper limits of the track fit quality parameters in the ITS ( $\chi_{\text{ITS}}^2/N_{\text{hits}}$ ) and in the TPC ( $\chi_{\text{TPC}}^2/N_{\text{clusters}}$ ) were varied in the ranges of 25–49 and 3–5, respectively. The maximum fraction of shared TPC clusters was varied between 0.2 to 1 and the maximum  $d_z$  was varied between 1 and 5 cm [41]. We have also quantified the impact of not including the ITS hit requirement in the track selection. The systematic uncertainty on the primary particle composition was estimated using a procedure similar to the one described in [41]. To quantify the uncertainty due to the imperfect simulation of the detector response, the track matching between the TPC and the ITS information in the data and in the simulation were compared. To achieve this, the fraction of secondary particles was rescaled according to fits to the measured DCA distributions. After this rescaling, the agreement between data and model was found to be within 3% for all collision systems. This value was assigned as an additional systematic uncertainty [41]. The systematic uncertainty on the secondary particle contamination considers the imperfection of the method (multi-component template fit) used to extract the correction. The fit ranges were varied and the fit was repeated using templates with two (primaries, secondaries) or three (primaries, secondaries from material, secondaries from weak decays) components. The maximum spread among these variations was assigned as the systematic uncertainty on the secondary contamination. This contribution dominates at low  $p_T$ . The density of materials

Table 1: Contributions to the relative (%) systematic uncertainty on the  $p_T$  spectra of primary charged particles in pp, p–Pb, and Pb–Pb collisions at  $\sqrt{s_{NN}} = 5.02$  TeV. Just for illustration, the range in the table corresponds to the lowest and highest relative systematic uncertainty in the considered  $p_T$  range. The individual contributions are summed in quadrature to obtain the total uncertainty.

Source of uncertainty	pp	p–Pb	Pb–Pb
Track selection	2.1–8.2	2.4–5.8	3.0–9.9
Particle composition	0.3–1.8	0.5–1.9	0.3–2.4
Secondary particles	0.0–0.4	0.0–2.4	0.0–1.9
Matching efficiency	2.0–4.2	0.7–3.7	0.6–3.7
Total	3.2–8.8	3.6–6.3	3.5–10.0
Total ( $N_{ch}$ -dependent)	2.0–4.5	1.7–4.0	1.1–3.7

used in simulations of the experimental setup was varied by  $\pm 4.5\%$  [35], resulting in a negligible systematic uncertainty in the considered  $p_T$  range of 0.5 to 6.0 GeV/ $c$ . For the estimation of total systematic uncertainty, all the above listed contributions were summed in quadrature. The systematic uncertainties are independent of the difference between the azimuthal angle of the associated particle and that of the trigger particle. The estimated systematic uncertainties on the  $p_T$  spectra significantly depend on  $p_T$ , while the dependence on the multiplicity classes is mild. The ranges of systematic uncertainties in the three considered collision systems are reported in Table 1 for the various sources described above.

### 3 Results and discussion

The  $p_T$  spectra measured in the transverse region for pp, p–Pb, and Pb–Pb collisions are shown in Fig. 2 (top panel). Results are presented for different multiplicity classes. The ratios between the spectra in the individual multiplicity classes and the MB (0–100%) one are shown in the bottom panel. In the  $p_T$  range 0.5 – 6 GeV/ $c$ , the ratios for the highest multiplicity classes (0–5% and 5–10%) are larger than unity and show an increasing trend with increasing  $p_T$  at low  $p_T$  ( $< 2 - 3$  GeV/ $c$ ) followed at higher  $p_T$  by a slow decrease. Instead, for the lowest multiplicity classes (40–60% and 60–90%) the ratios are lower than unity and follow an opposite trend with  $p_T$ , decreasing at low  $p_T$  and increasing for  $p_T > 3$  GeV/ $c$ . The behaviour of the ratios as a function of the event activity is reminiscent of analogous ratios as a function of the number of MPI in pp collisions simulated with PYTHIA 8, including colour reconnection [50]. It was not observed before in data because, in contrast to the present analysis, the jet contribution was included in the  $p_T$  spectra [44].

The top (bottom) panel of Fig. 3 shows the charged particle yields for the toward (away) region after the subtraction of the yields measured in the transverse region in pp, p–Pb and Pb–Pb collisions. Results are compared with the  $p_T$  spectra measured for MB pp collisions (0–100% V0M pp event class) quantified with the ratio  $I_X^{t,a}$ , as defined in Eq. 1. At low transverse momenta,  $p_T < 4$  GeV/ $c$ ,  $I_X^{t,a}$  is consistent with unity in pp and p–Pb collisions. In contrast,  $I_X^{t,a}$  in Pb–Pb collisions exhibits a strong multiplicity dependence over the whole measured  $p_T$  interval. The  $I_X^{t,a}$  magnitude is larger for semi-peripheral Pb–Pb collisions, the maximum is observed for 20–40% Pb–Pb collisions, and is smaller for the most central and most peripheral classes. Given that the  $v_2$  contribution is not subtracted from the jet-like yields reported in Fig. 3, the centrality dependence of  $I_X^{t,a}$  follows the behaviour of  $v_2$  as a function of collision centrality and particle  $p_T$  in Pb–Pb collisions at LHC energies [51].

Figure 4 shows the measured values of  $I_X^{t,a}$  in the transverse momentum interval  $4 < p_T < 6$  GeV/ $c$  as a function of the average multiplicity in the transverse region for all the multiplicity classes considered in pp, p–Pb and Pb–Pb collisions. The figure shows that, within uncertainties, the  $I_X^{t,a}$  values are close to unity for all the multiplicity classes measured in pp and p–Pb collisions. This indicates that effects induced by possible energy loss in these systems are not observed within uncertainties. This

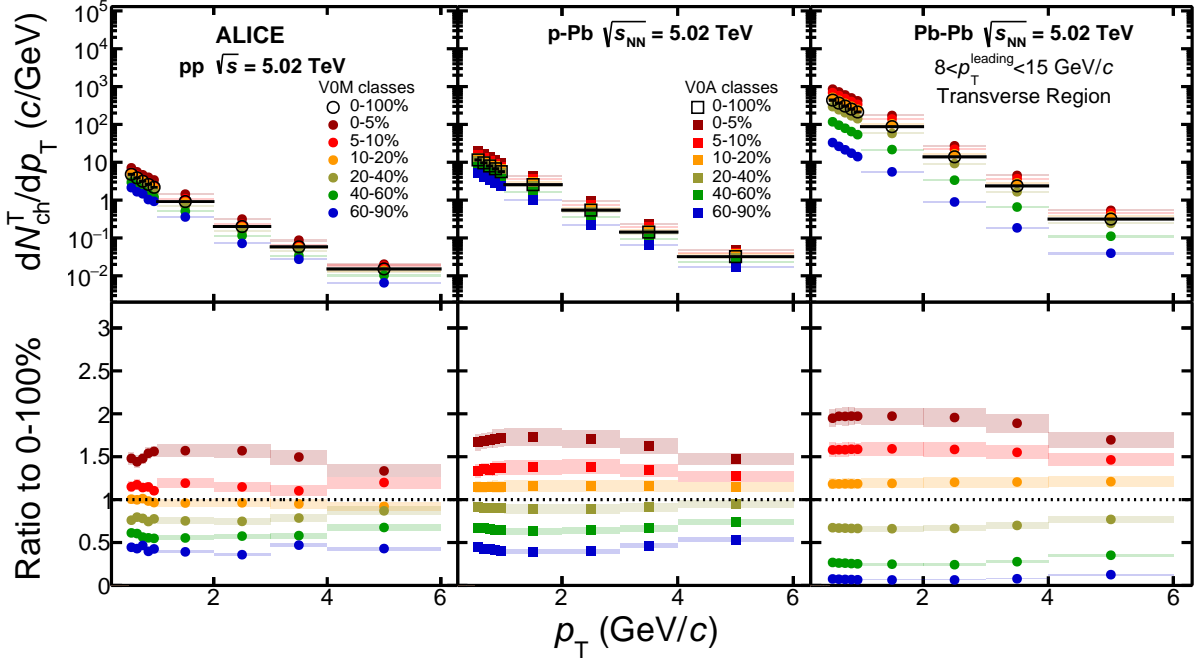


Figure 2: (colour online) Top panel:  $p_T$  spectra of charged particles in the transverse region for different multiplicity classes in pp (left), p-Pb (middle) and Pb-Pb (right) collisions at  $\sqrt{s_{NN}} = 5.02$  TeV. Lower panel: Ratio of  $p_T$  spectra in different multiplicity classes to  $p_T$  spectrum in 0-100% multiplicity class for the corresponding collision systems. The statistical and systematic uncertainties are shown by bars and boxes, respectively.

result is consistent with previous studies of nuclear modification factor [33] and hadron-jet recoil measurements [34]. By contrast, for Pb-Pb collisions the  $I_X^{t,a}$  values are compatible to unity for peripheral collisions, and show a gradual enhancement (reduction) with the increase in multiplicity for the toward (away) region. The behaviour is the same for the  $I_X^{t,a}$  values measured either assuming a flat background or a  $v_2$ -modulated background. The  $v_2$ -modulated background was estimated following the approach depicted in Eq. 2 and using the  $v_2$  data reported in [48]. This behaviour is qualitatively similar to the di-hadron correlation results reported by the STAR and ALICE collaborations [29, 30]. Given that  $I_X^{t,a}$  is sensitive to the same effects as  $I_{AA}$ , the interpretation of the results is similar to that reported in [30]. On one hand, the suppression in the away region is expected from the strong in-medium energy loss; on the other hand, the enhancement observed in the toward region is also subject to medium effects. The ratio is sensitive to a) a possible change of the fragmentation functions, b) a possible modification of the quark to gluon jet ratio in the final state due to different coupling with medium, and c) a possible bias on the parton spectrum due to trigger particle selection. It is likely that all three effects play a role [30]. A detailed quantification of the contribution of each effect is beyond the scope of the present paper.

In order to get further insight into the effect, the measured  $I_X^{t,a}$  values are compared in Fig. 5 with model predictions. For high-multiplicity pp collisions, although  $I_X^{t,a}$  is close to unity, a small trend with multiplicity is visible, which is not seen at similar multiplicities (20-90% V0A) in p-Pb data. To understand the source of these slight deviations from unity, the data are compared with the predictions from the PYTHIA 8 (Monash tune [28]) and EPOS-LHC [21] event generators. In PYTHIA, the hadronization of quarks is simulated using the Lund string fragmentation model [52]. Various PYTHIA tunes have been developed through extensive comparison of Monte Carlo distributions with the minimum bias data from different experiments. The Monash tune of PYTHIA 8 is tuned to LHC data and uses an updated set of hadronization parameters compared to the previous tunes [28]. EPOS-LHC is built on the Parton-Based Gribov Regge Theory. Utilising the colour exchange mechanism of string excitation, the model is tuned

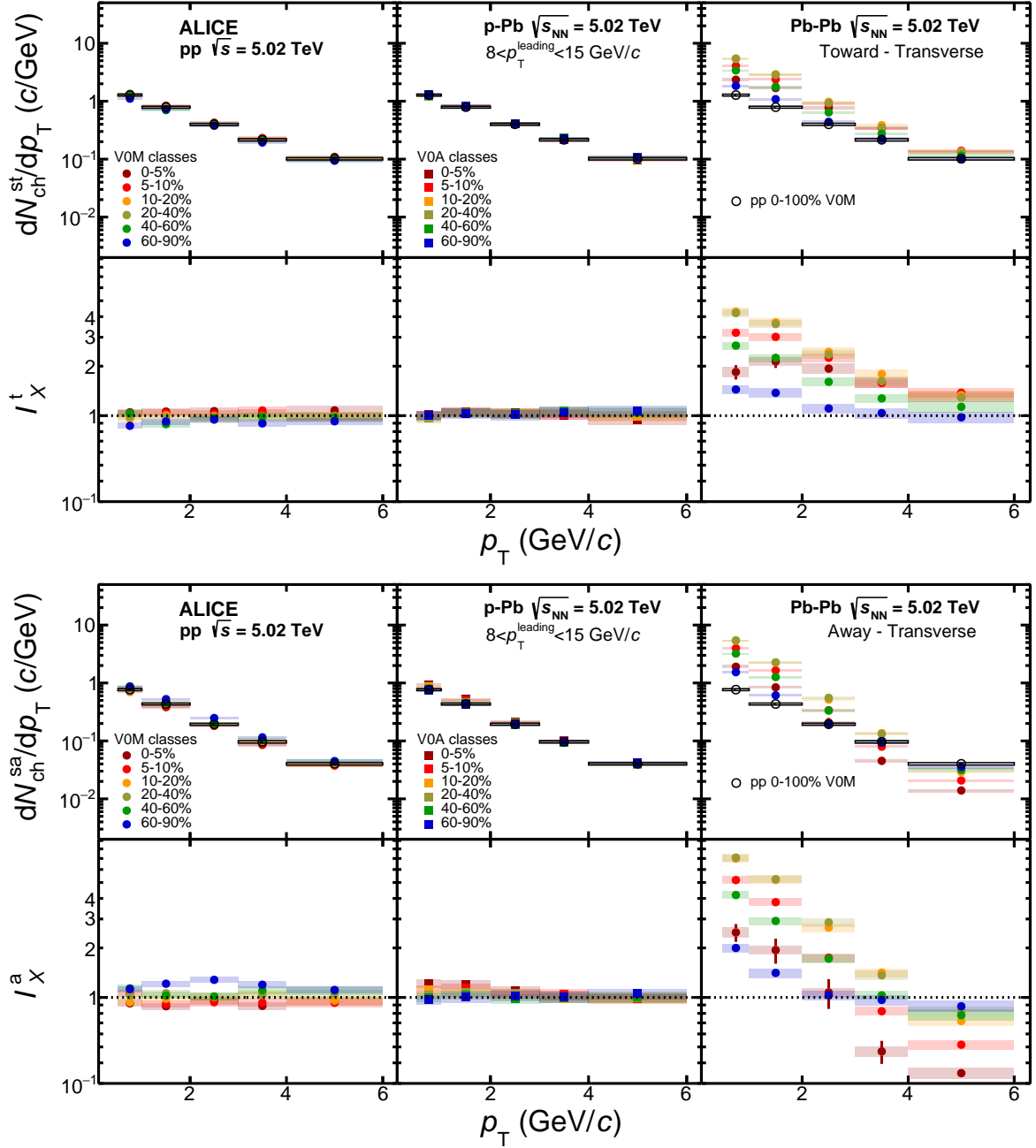


Figure 3: (colour online)  $p_T$  spectra of charged particles in Toward-Transverse,  $dN_{\text{ch}}^{\text{st}}/dp_T$  (top plot) and Away-Transverse,  $dN_{\text{ch}}^{\text{sa}}/dp_T$  (bottom plot) regions for different multiplicity classes in pp (left), p-Pb (middle) and Pb-Pb (right) collisions at  $\sqrt{s_{\text{NN}}} = 5.02$  TeV. The lower panels of both plots show the ratio to minimum bias pp collisions. The statistical and systematic uncertainties are shown by bars and boxes, respectively.

to LHC data [21]. In this model, a part of the collision system which has high parton densities becomes a “core” region that evolves hydrodynamically as a quark–gluon plasma and it is surrounded by a more dilute “corona” for which fragmentation occurs in the vacuum. The upper panel of Fig. 5 shows  $I_X^{t,a}$  for different multiplicity classes. The observed deviations from unity are reproduced by PYTHIA 8 for both the toward and away regions. Given that PYTHIA 8 does not incorporate any jet quenching mechanism, the origin of the effect in high  $\langle N_{\text{ch}}^T \rangle$  collisions is related to a remaining bias towards harder fragmentation and more activity from initial and final state radiation [53]. These effects enhance the high- $p_T$  yield



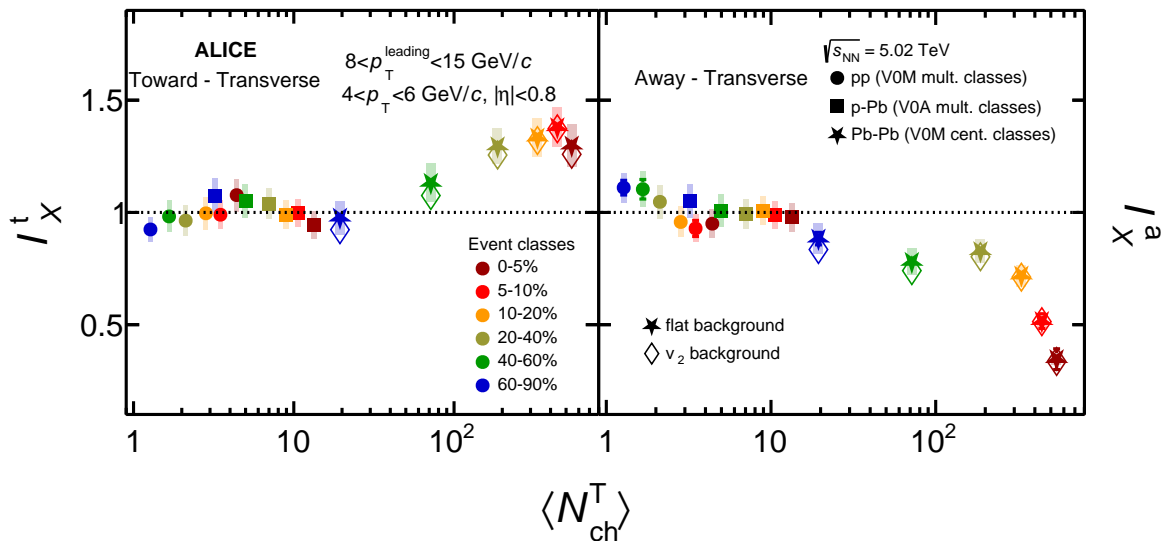


Figure 4: (colour online) The  $I_X^t$  (left) and  $I_X^a$  (right) as a function of  $\langle N_{ch}^T \rangle$  in  $4 < p_T < 6$  GeV/c for different multiplicity classes in pp, p-Pb and Pb-Pb collisions at  $\sqrt{s_{NN}} = 5.02$  TeV. Pb-Pb results are shown assuming a flat background (filled markers), and assuming a  $v_2$ -modulated background (empty markers). The statistical and systematic uncertainties are shown by bars and boxes, respectively.

in the toward region, and produce a broadening in the away region [54]. The EPOS-LHC results in the away region are similar to both data and PYTHIA 8. However, for  $I_X^t$  EPOS-LHC exhibits a trend with a maximum at intermediate multiplicity and a reduction toward low and high multiplicities, which is not consistent with the measurements.

The middle and bottom panels of Fig. 5 show  $I_X^{t,a}$  measured for p-Pb and Pb-Pb collisions, respectively. The data are compared to PYTHIA 8/Angantyr [55] and EPOS-LHC predictions. The Angantyr model in PYTHIA 8 extrapolates the dynamics from pp collisions to p-Pb and Pb-Pb collisions, generalising the formalism adopted for pp collisions by including a description of the nucleon positions within the colliding nuclei and utilising the Glauber model to calculate the number of interacting nucleons and binary nucleon-nucleon collisions. PYTHIA 8/Angantyr, which does not include jet quenching effects, predicts  $I_X^a$  values consistent with unity for all the multiplicity classes in Pb-Pb collisions. Whereas for p-Pb collisions  $I_X^a$  is consistent with unity, and  $I_X^t$  is slightly below unity. In EPOS-LHC, a certain  $p_T$  cutoff is defined in such a way that, above this cutoff, a particle loses part of its momentum in the core but survives as an independent particle produced by a flux tube. Soft particles, which are below the  $p_T$  cutoff, get completely absorbed and form the core. This sort of energy loss mechanism implemented in EPOS-LHC depends on the system size [21, 56, 57]. Figure 5 (middle) shows that for p-Pb collisions, EPOS-LHC does not describe either the magnitude or the trend of the multiplicity dependence of the measured ratio in the toward region,  $I_X^t$ . However, the model is in reasonable agreement with data in the away region. For Pb-Pb collisions, EPOS-LHC predicts a significant enhancement of  $I_X^{t,a}$  for low  $\langle N_{ch}^T \rangle$  ranges and deviates significantly from the experimental results. In summary, while the data from Pb-Pb collisions are in agreement with expectations from parton energy loss due to the presence of a hot and dense medium, pp and p-Pb data do not show any hint of medium effects in the multiplicity range which is reported.

## 4 Summary

The transverse momentum spectra ( $0.5 \leq p_T < 6$  GeV/c) of primary charged particles in three azimuthal regions (toward, away and transverse) defined with respect to the direction of the particle with the highest

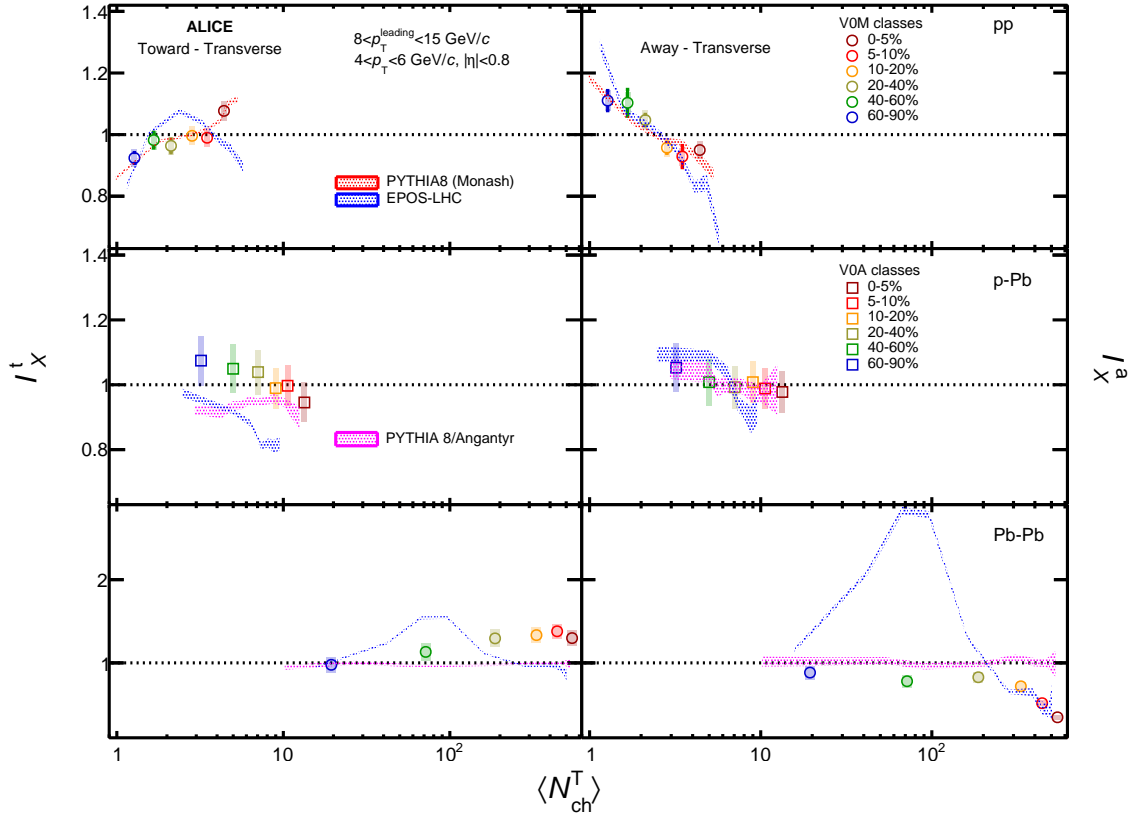


Figure 5: (colour online) Comparison of the measured the  $I_X^t$  (left) and  $I_X^a$  (right) in  $4 < p_T < 6$  GeV/ $c$  with model predictions. The results are shown as a function of  $\langle N_{ch}^T \rangle$  for different multiplicity classes in pp (top panel), p-Pb (middle panel) and Pb-Pb (bottom panel) collisions at  $\sqrt{s_{NN}} = 5.02$  TeV. The red and magenta lines show the PYTHIA 8 (Monash) [28] and PYTHIA 8/Angantyr [28] predictions, respectively. The blue lines show the EPOS-LHC [21] results. The statistical and systematic uncertainties are shown by bars and boxes, respectively.

transverse momentum in the event ( $8 \leq p_T^{\text{trig}} < 15$  GeV/ $c$ ) are reported. The spectra are studied as a function of the multiplicity measured at forward pseudorapidities for pp, p-Pb, and Pb-Pb collisions at  $\sqrt{s_{NN}} = 5.02$  TeV. The  $p_T$  spectra in the transverse region are subtracted from those of the away and toward regions. This is based on the assumption that the transverse side provides a good estimation of the underlying event contribution in both the toward and away regions. However, for the interpretation of the results one has to keep in mind that  $v_2$  modulates the background and this effect is important for semi-central Pb-Pb collisions and for  $p_T > 4$  GeV/ $c$  the effect is less than 5% in central and peripheral Pb-Pb collisions. Ratios to MB pp ( $I_X^{t,a}$ ), i.e., the multiplicity dependent yields normalised to the yield measured in MB pp collisions, are reported. At low transverse momentum ( $p_T < 3$  GeV/ $c$ ), within uncertainties, the  $I_X^{t,a}$  values are multiplicity independent for both the toward and away regions. In contrast, in Pb-Pb collisions for both toward and away regions the  $I_X^{t,a}$  values exhibit a centrality dependence which is expected given the residual presence of elliptic flow. In the highest transverse momentum interval ( $4 < p_T < 6$  GeV/ $c$ ), the  $I_X^{t,a}$  values in p-Pb collisions are closer to unity for the 60% highest-multiplicity (most central) Pb-Pb collisions. The  $I_X^a$  ( $I_X^t$ ) values exhibit a small reduction (increase) towards high V0 activity in pp collisions. This trend is well reproduced by PYTHIA 8. In the model, it is due to a selection bias towards pp collisions with harder fragmentation and larger activity from initial and final state radiation. For p-Pb collisions, within uncertainties, the  $I_X^{t,a}$  values are consistent with unity and do not show a multiplicity dependence. PYTHIA 8/Angantyr fairly describes  $I_X^a$ , but it underestimates by about 10% the  $I_X^t$  values in the low multiplicity classes (40-90% VOA event class). For Pb-Pb collisions, the  $I_X^{t,a}$  values are close to unity for peripheral collisions, and show a gradual increase (reduction) in the toward

(away) region with increasing multiplicity. A similar observable,  $I_{AA}$ , based on the per-trigger yield of associated particles in di-hadron correlation has been studied for central and peripheral Pb–Pb collisions at  $\sqrt{s_{NN}} = 2.76$  TeV. The behaviour of  $I_X^{t,a}$  exhibits the same features as  $I_{AA}$ : in central collisions, on the away-side, a suppression is observed as expected from strong in-medium energy loss. In the toward region, an enhancement is observed. PYTHIA 8/Angantyr predicts  $I_X^{t,a} \approx 1$  for all multiplicity intervals, and it does not reproduce the observed away-side suppression or toward-side enhancement. Generally, EPOS-LHC does not describe the measured  $I_X^{t,a}$  ratios.

In summary, within the multiplicity reach reported in this paper, no jet quenching effects are observed in pp and p–Pb collisions within uncertainties. Further studies are required to extend the present analysis to higher multiplicities, which are currently limited by the event selection based on the forward V0 detector. The analysis of future pp and p–Pb collisions with much larger integrated luminosity may remove this limitation.

## References

- [1] T. Sjöstrand and M. van Zijl, “A Multiple Interaction Model for the Event Structure in Hadron Collisions”, *Phys. Rev. D* **36** (1987) 2019.
- [2] P. Bartalini and J. R. Gaunt, eds., *Multiple Parton Interactions at the LHC*, vol. 29. WSP, 2019.
- [3] **CDF** Collaboration, T. Affolder *et al.*, “Charged Jet Evolution and the Underlying Event in  $p\bar{p}$  Collisions at 1.8 TeV”, *Phys. Rev. D* **65** (2002) 092002.
- [4] **STAR** Collaboration, J. Adam *et al.*, “Underlying event measurements in  $p + p$  collisions at  $\sqrt{s} = 200$  GeV at RHIC”, *Phys. Rev. D* **101** no. 5, (2020) 052004, arXiv:1912.08187 [nucl-ex].
- [5] C. M. Buttar *et al.*, “The Underlying Event”, in *HERA and the LHC: A Workshop on the Implications of HERA for LHC Physics: CERN - DESY Workshop 2004/2005 (Midterm Meeting, CERN, 11-13 October 2004; Final Meeting, DESY, 17-21 January 2005)*. CERN, Geneva, 12, 2005.
- [6] **STAR** Collaboration, J. Adams *et al.*, “Experimental and theoretical challenges in the search for the quark gluon plasma: The STAR Collaboration’s critical assessment of the evidence from RHIC collisions”, *Nucl. Phys. A* **757** (2005) 102–183, arXiv:nucl-ex/0501009.
- [7] **PHENIX** Collaboration, K. Adcox *et al.*, “Formation of dense partonic matter in relativistic nucleus-nucleus collisions at RHIC: Experimental evaluation by the PHENIX collaboration”, *Nucl. Phys. A* **757** (2005) 184–283, arXiv:nucl-ex/0410003.
- [8] Busza, Wit and Rajagopal, Krishna and van der Schee, Wilke, “Heavy Ion Collisions: The Big Picture, and the Big Questions”, *Ann. Rev. Nucl. Part. Sci.* **68** (2018) 339–376, arXiv:1802.04801 [hep-ph].
- [9] J. L. Nagle and W. A. Zajc, “Small System Collectivity in Relativistic Hadronic and Nuclear Collisions”, *Ann. Rev. Nucl. Part. Sci.* **68** (2018) 211–235, arXiv:1801.03477 [nucl-ex].
- [10] A. Ortiz, P. Christiansen, E. Cuautle Flores, I. Maldonado Cervantes, and G. Paić, “Color Reconnection and Flowlike Patterns in  $pp$  Collisions”, *Phys. Rev. Lett.* **111** no. 4, (2013) 042001, arXiv:1303.6326 [hep-ph].
- [11] C. Bierlich, G. Gustafson, L. Lönnblad, and A. Tarasov, “Effects of Overlapping Strings in pp Collisions”, *JHEP* **03** (2015) 148, arXiv:1412.6259 [hep-ph].

- [12] C. Bierlich, S. Chakraborty, G. Gustafson, and L. Lönnblad, “Setting the string shoving picture in a new frame”, *JHEP* **03** (2021) 270, arXiv:2010.07595 [hep-ph].
- [13] T. Sjöstrand, S. Ask, J. R. Christiansen, R. Corke, N. Desai, P. Ilten, S. Mrenna, S. Prestel, C. O. Rasmussen, and P. Z. Skands, “An introduction to PYTHIA 8.2”, *Comput. Phys. Commun.* **191** (2015) 159–177, arXiv:1410.3012 [hep-ph].
- [14] ALICE Collaboration, J. Adam *et al.*, “Enhanced production of multi-strange hadrons in high-multiplicity proton-proton collisions”, *Nature Phys.* **13** (2017) 535–539, arXiv:1606.07424 [nucl-ex].
- [15] ALICE Collaboration, J. Adam *et al.*, “Multiplicity dependence of charged pion, kaon, and (anti)proton production at large transverse momentum in p-Pb collisions at  $\sqrt{s_{NN}} = 5.02$  TeV”, *Phys. Lett. B* **760** (2016) 720–735, arXiv:1601.03658 [nucl-ex].
- [16] ALICE Collaboration, S. Acharya *et al.*, “Multiplicity dependence of light-flavor hadron production in pp collisions at  $\sqrt{s} = 7$  TeV”, *Phys. Rev. C* **99** no. 2, (2019) 024906, arXiv:1807.11321 [nucl-ex].
- [17] CMS Collaboration, V. Khachatryan *et al.*, “Observation of Long-Range Near-Side Angular Correlations in Proton-Proton Collisions at the LHC”, *JHEP* **09** (2010) 091, arXiv:1009.4122 [hep-ex].
- [18] CMS Collaboration, V. Khachatryan *et al.*, “Evidence for collectivity in pp collisions at the LHC”, *Phys. Lett. B* **765** (2017) 193–220, arXiv:1606.06198 [nucl-ex].
- [19] T. Martin, P. Skands, and S. Farrington, “Probing Collective Effects in Hadronisation with the Extremes of the Underlying Event”, *Eur. Phys. J. C* **76** no. 5, (2016) 299, arXiv:1603.05298 [hep-ph].
- [20] ALICE Collaboration, S. Acharya *et al.*, “Underlying Event properties in pp collisions at  $\sqrt{s} = 13$  TeV”, *JHEP* **04** (2020) 192, arXiv:1910.14400 [nucl-ex].
- [21] T. Pierog, I. Karpenko, J. M. Katzy, E. Yatsenko, and K. Werner, “EPOS LHC: Test of collective hadronization with data measured at the CERN Large Hadron Collider”, *Phys. Rev. C* **92** no. 3, (2015) 034906, arXiv:1306.0121 [hep-ph].
- [22] J. Bellm *et al.*, “Herwig 7.0/Herwig++ 3.0 release note”, *Eur. Phys. J. C* **76** no. 4, (2016) 196, arXiv:1512.01178 [hep-ph].
- [23] M. Strikman, “Transverse Nucleon Structure and Multiparton Interactions”, *Acta Phys. Polon. B* **42** (2011) 2607–2630, arXiv:1112.3834 [hep-ph].
- [24] A. Ortiz and L. Valencia Palomo, “Probing color reconnection with underlying event observables at the LHC energies”, *Phys. Rev. D* **99** no. 3, (2019) 034027, arXiv:1809.01744 [hep-ex].
- [25] ALICE Collaboration, J. Adam *et al.*, “Centrality dependence of particle production in p-Pb collisions at  $\sqrt{s_{NN}} = 5.02$  TeV”, *Phys. Rev. C* **91** no. 6, (2015) 064905, arXiv:1412.6828 [nucl-ex].
- [26] C. Loizides and A. Morsch, “Absence of jet quenching in peripheral nucleus–nucleus collisions”, *Phys. Lett. B* **773** (2017) 408–411, arXiv:1705.08856 [nucl-ex].
- [27] ALICE Collaboration, S. Acharya *et al.*, “Analysis of the apparent nuclear modification in peripheral Pb–Pb collisions at 5.02 TeV”, *Phys. Lett. B* **793** (2019) 420–432, arXiv:1805.05212 [nucl-ex].

- [28] P. Skands, S. Carrazza, and J. Rojo, “Tuning PYTHIA 8.1: the Monash 2013 Tune”, *Eur. Phys. J. C* **74** no. 8, (2014) 3024, arXiv:1404.5630 [hep-ph].
- [29] **STAR** Collaboration, J. Adams *et al.*, “Direct observation of dijets in central Au+Au collisions at  $\sqrt{s_{NN}} = 200$  GeV”, *Phys. Rev. Lett.* **97** (2006) 162301, arXiv:nucl-ex/0604018.
- [30] **ALICE** Collaboration, K. Aamodt *et al.*, “Particle-yield modification in jet-like azimuthal di-hadron correlations in Pb-Pb collisions at  $\sqrt{s_{NN}} = 2.76$  TeV”, *Phys. Rev. Lett.* **108** (2012) 092301, arXiv:1110.0121 [nucl-ex].
- [31] **ALICE** Collaboration, J. Adam *et al.*, “Jet-like correlations with neutral pion triggers in pp and central Pb-Pb collisions at 2.76 TeV”, *Phys. Lett. B* **763** (2016) 238–250, arXiv:1608.07201 [nucl-ex].
- [32] G.-Y. Qin and X.-N. Wang, “Jet quenching in high-energy heavy-ion collisions”, *Int. J. Mod. Phys. E* **24** no. 11, (2015) 1530014, arXiv:1511.00790 [hep-ph].
- [33] **ALICE** Collaboration, S. Acharya *et al.*, “Transverse momentum spectra and nuclear modification factors of charged particles in pp, p-Pb and Pb-Pb collisions at the LHC”, *JHEP* **11** (2018) 013, arXiv:1802.09145 [nucl-ex].
- [34] **ALICE** Collaboration, S. Acharya *et al.*, “Constraints on jet quenching in p-Pb collisions at  $\sqrt{s_{NN}} = 5.02$  TeV measured by the event-activity dependence of semi-inclusive hadron-jet distributions”, *Phys. Lett. B* **783** (2018) 95–113, arXiv:1712.05603 [nucl-ex].
- [35] **ALICE** Collaboration, B. B. Abelev *et al.*, “Performance of the ALICE Experiment at the CERN LHC”, *Int. J. Mod. Phys. A* **29** (2014) 1430044, arXiv:1402.4476 [nucl-ex].
- [36] **ALICE** Collaboration, K. Aamodt *et al.*, “The ALICE experiment at the CERN LHC”, *JINST* **3** (2008) S08002.
- [37] **ALICE** Collaboration, S. Acharya *et al.*, “Multiplicity dependence of (multi-)strange hadron production in proton-proton collisions at  $\sqrt{s} = 13$  TeV”, *Eur. Phys. J. C* **80** no. 2, (2020) 167, arXiv:1908.01861 [nucl-ex].
- [38] **ALICE** Collaboration, J. Adam *et al.*, “Centrality dependence of the charged-particle multiplicity density at midrapidity in Pb-Pb collisions at  $\sqrt{s_{NN}} = 5.02$  TeV”, *Phys. Rev. Lett.* **116** no. 22, (2016) 222302, arXiv:1512.06104 [nucl-ex].
- [39] **ALICE** Collaboration, J. Adam *et al.*, “Centrality dependence of particle production in p-Pb collisions at  $\sqrt{s_{NN}} = 5.02$  TeV”, *Phys. Rev. C* **91** no. 6, (2015) 064905, arXiv:1412.6828 [nucl-ex].
- [40] **ALICE** Collaboration, “The ALICE definition of primary particles”, *ALICE-PUBLIC-2017-005* (Jun, 2017). <https://cds.cern.ch/record/2270008>.
- [41] **ALICE** Collaboration, S. Acharya *et al.*, “Transverse momentum spectra and nuclear modification factors of charged particles in pp, p-Pb and Pb-Pb collisions at the LHC”, *JHEP* **11** (2018) 013, arXiv:1802.09145 [nucl-ex].
- [42] **ALICE** Collaboration, *ALICE time projection chamber: Technical Design Report*. Technical design report. ALICE. CERN, Geneva, 2000. <http://cds.cern.ch/record/451098>.
- [43] **ALICE** Collaboration, B. Abelev *et al.*, “Centrality Dependence of Charged Particle Production at Large Transverse Momentum in Pb-Pb Collisions at  $\sqrt{s_{NN}} = 2.76$  TeV”, *Phys. Lett. B* **720** (2013) 52–62, arXiv:1208.2711 [hep-ex].

- [44] **ALICE** Collaboration, S. Acharya *et al.*, “Charged-particle production as a function of multiplicity and transverse sphericity in pp collisions at  $\sqrt{s} = 5.02$  and 13 TeV”, *Eur. Phys. J. C* **79** no. 10, (2019) 857, arXiv:1905.07208 [nucl-ex].
- [45] R. Brun, F. Bruyant, F. Carminati, S. Giani, M. Maire, A. McPherson, G. Patrick, and L. Urban, *GEANT: Detector Description and Simulation Tool; Oct 1994*. CERN Program Library. CERN, Geneva, 1993. <https://cds.cern.ch/record/1082634>. Long Writeup W5013.
- [46] W.-T. Deng, X.-N. Wang, and R. Xu, “Hadron production in p+p, p+Pb, and Pb+Pb collisions with the HIJING 2.0 model at energies available at the CERN Large Hadron Collider”, *Phys. Rev. C* **83** (2011) 014915, arXiv:1008.1841 [hep-ph].
- [47] **ALICE** Collaboration, K. Aamodt *et al.*, “Harmonic decomposition of two-particle angular correlations in Pb-Pb collisions at  $\sqrt{s_{NN}} = 2.76$  TeV”, *Phys. Lett. B* **708** (2012) 249–264, arXiv:1109.2501 [nucl-ex].
- [48] **ALICE** Collaboration, B. Abelev *et al.*, “Anisotropic flow of charged hadrons, pions and (anti-)protons measured at high transverse momentum in Pb-Pb collisions at  $\sqrt{s_{NN}}=2.76$  TeV”, *Phys. Lett. B* **719** (2013) 18–28, arXiv:1205.5761 [nucl-ex].
- [49] G. D’Agostini, “A Multidimensional unfolding method based on Bayes’ theorem”, *Nucl. Instrum. Meth. A* **362** (1995) 487–498.
- [50] A. Ortiz, A. Paz, J. D. Romo, S. Tripathy, E. A. Zepeda, and I. Bautista, “Multiparton interactions in pp collisions from machine learning-based regression”, *Phys. Rev. D* **102** no. 7, (2020) 076014, arXiv:2004.03800 [hep-ph].
- [51] **ALICE** Collaboration, J. Adam *et al.*, “Anisotropic flow of charged particles in Pb-Pb collisions at  $\sqrt{s_{NN}} = 5.02$  TeV”, *Phys. Rev. Lett.* **116** no. 13, (2016) 132302, arXiv:1602.01119 [nucl-ex].
- [52] B. Andersson, G. Gustafson, G. Ingelman, and T. Sjostrand, “Parton Fragmentation and String Dynamics”, *Phys. Rept.* **97** (1983) 31–145.
- [53] G. Bencedi, A. Ortiz, and A. Paz, “Disentangling the hard gluon bremsstrahlung effects from the relative transverse activity classifier in pp collisions”, *Phys. Rev. D* **104** no. 1, (2021) 016017, arXiv:2105.04838 [hep-ph].
- [54] G. Bencédi, A. Ortiz, and S. Tripathy, “Apparent modification of the jet-like yield in proton-proton collisions with large underlying event”, *J. Phys. G* **48** no. 1, (2020) 015007, arXiv:2007.03857 [hep-ph].
- [55] C. Bierlich, G. Gustafson, L. Lönnblad, and H. Shah, “The Angantyr model for Heavy-Ion Collisions in PYTHIA8”, *JHEP* **10** (2018) 134, arXiv:1806.10820 [hep-ph].
- [56] R. Baier, Y. L. Dokshitzer, A. H. Mueller, S. Peigne, and D. Schiff, “Radiative energy loss of high-energy quarks and gluons in a finite volume quark - gluon plasma”, *Nucl. Phys. B* **483** (1997) 291–320, arXiv:hep-ph/9607355.
- [57] S. Peigne, “Collisional Energy Loss of a Fast Parton in a QGP”, *AIP Conf. Proc.* **1038** no. 1, (2008) 139–148, arXiv:0806.0242 [hep-ph].